atmosphere

MDPI

Article

Composition and Reactivity of Volatile Organic Compounds and the Implications for Ozone Formation in the North China Plain

Saimei Hao [1,2], Qiyue Du [3], Xiaofeng Wei [2], Huaizhong Yan [4], Miao Zhang [4], Youmin Sun [2], Shijie Liu [5], Lianhuan Fan [2] and Guiqin Zhang [2,*]

1 Qingdao Gemini Scientific Co., Ltd., Qingdao 266100, China; 2020040209@stu.sdjzu.edu.cn
2 School of Municipal and Environmental Engineering, Shandong Jianzhu University, Jinan 250101, China; weixf@sdjzu.edu.cn (X.W.); ymsun@sdjzu.edu.cn (Y.S.); 2021040205@stu.sdjzu.edu.cn (L.F.)
3 School of Safety and Environmental Engineering, Shandong University of Science and Technology, Qingdao 266555, China; dqy-061@sdust.edu.cn
4 Shandong Provincial Ecological Environment Monitoring Center, Jinan 250101, China; yanhuaizhong@shandong.cn (H.Y.); zhangmiao@shandong.cn (M.Z.)
5 Resource and Environment Innovation Institute, Shandong Jianzhu University, Jinan 250101, China; liushijie23@sdjzu.edu.cn
* Correspondence: zhangguiqin@sdjzu.edu.cn; Tel.: +86-136-7541-1301

Abstract: Enhanced ozone (O_3) pollution has emerged as a pressing environmental concern in China, particularly for densely populated megacities and major city clusters. However, volatile organic compounds (VOCs), the key precursors to O_3 formation, have not been routinely measured. In this study, we characterize the spatial and temporal patterns of VOCs and examine the role of VOCs in O_3 production in five cities (Dongying (DY), Rizhao (RZ), Yantai (YT), Weihai (WH), and Jinan (JN)) in the North China Plain (NCP) for two sampling periods (June and December) in 2021 through continuous field observations. Among various VOC categories, alkanes accounted for the largest proportion of VOCs in the cities. For VOCs, chemical reactivities, aromatic hydrocarbons, and alkenes were dominant contributors to O_3 formation potential (OFP). Unlike inland regions, the contribution to OFP from OVOCs increased greatly at high O_3 concentrations in coastal regions (especially YT). Model simulations during the O_3 episode show that the net O_3 production rates were 27.87, 10.24, and 10.37 ppbv/h in DY, RZ, and JN. The pathway of HO_2 + NO contributed the most to O_3 production in JN and RZ, while RO_2 + NO was the largest contributor to O_3 production in DY. The relative incremental reactivity (RIR) revealed that O_3 formation in DY was the transitional regime, while it was markedly the VOC-limited regime in JN and RZ. The O_3 production response is influenced by NOx concentration and has a clear daily variation pattern (the sensitivity is greater from 15:00 to 17:00). The most efficiencies in O_3 reduction could be achieved by reducing NOx when the NOx concentration is low (less than 20 ppbv in this study). This study reveals the importance of ambient VOCs in O_3 production over the NCP and demonstrates that a better grasp of VOC sources and profiles is critical for in-depth O_3 regulation in the NCP.

Keywords: volatile organic compounds (VOCs); O_3 pollution; ozone formation potential (OFP); observation-based model (OBM)

Citation: Hao, S.; Du, Q.; Wei, X.; Yan, H.; Zhang, M.; Sun, Y.; Liu, S.; Fan, L.; Zhang, G. Composition and Reactivity of Volatile Organic Compounds and the Implications for Ozone Formation in the North China Plain. *Atmosphere* **2024**, *15*, 213. https://doi.org/10.3390/atmos15020213

Academic Editor: Tao Zhu

Received: 3 January 2024
Revised: 30 January 2024
Accepted: 5 February 2024
Published: 9 February 2024

1. Introduction

Tropospheric ozone (O_3) is a secondary pollutant that forms through the photooxidation of precursors in the presence of sunlight. Elevated O_3 levels greatly contribute to the degradation of regional air quality [1]. Exposure to high O_3 levels has been linked to detrimental health effects including cardiovascular diseases, respiratory infections, and neurodevelopment disruptions [2,3]. Over the past decade, major city clusters in China have been suffering from elevated O_3 pollution, with high rates of morbidity and mortality

related to O_3 exposure. In addition to adverse health outcomes, high O_3 levels are detrimental to plants and crops through reducing the carbon sequestration of vegetation [4,5].

The regulation of O_3 pollution is challenging due to the non-linear relationship between O_3 and its precursors (including volatile organic compounds (VOCs) and nitrogen oxides (NOx)) [6]. The chemical composition and sources of VOCs are complex and varied [7]. Generally, VOCs were divided into six types, namely alkanes, alkenes, alkynes, aromatic hydrocarbons, halogenated hydrocarbons, and oxygenated VOCs (OVOCs). The spatial distribution of VOCs throughout China has been extensively investigated in previous studies [8,9]. Alkanes have been widely identified as the dominant VOCs in northern China [10], and OVOCs predominate in the hilly regions of southeast China [11]. Furthermore, it was reported that higher aromatic hydrocarbon levels were depicted in Shanghai due to substantial solvent usage [12]. Despite the abovementioned extensive studies on the identification of dominant VOC species and source apportionment of VOCs, the sources of ambient VOCs in northern China remain poorly understood.

Northern China has been identified as a highly polluted area affected by frequent O_3 episodes [13]. In particular, densely populated cities in the Shandong Peninsula have suffered high levels of O_3 exposure and act as receptors of regional O_3 air mass under synoptic patterns. However, less attention has been paid to this region and limited prior work is insufficient for elucidating O_3 formation over the Shandong Peninsula. Therefore, it is critical to investigate the spatial and temporal pattern of ambient VOCs across this region and examine the chemical reactivity of VOCs among cities in the Shandong Peninsula. In 2021, field measurements of VOCs were conducted at five cities within the Shandong Peninsula, including Jinan (JN), Dongying (DY), Rizhao (RZ), Yantai (YT), and Weihai (WH). DY, RZ, YT, and WH are coastal cities located in the eastern Shandong Peninsula, and DY has urban O_3 precursor emissions in close proximity to industrial sectors (oil field extraction) [14]. As the capital city of Shandong Province, Jinan (JN) is a typical city which experienced severe O_3 pollution under the transport pathway in northern China [15]. The detailed measurements for these cities are expected to shape a clear map of VOC composition and shed further light on the development of effective O_3 regulation policies.

In this study, we combine field measurements and box modeling to characterize the sources of VOCs and identify the influence of VOC emissions on O_3 production in the Shandong Peninsula. The composition and temporal pattern of ambient VOCs was sampled and analyzed in five cities in the Shandong Peninsula for the periods of June and December 2021. The chemical reactivity of VOCs was calculated by means of the maximum incremental reactivity method (MIR). Furthermore, box modeling was performed using the MCM model for investigating O_3 production pathways in coastal and inland cities in summer, and key VOC species affecting O_3 production were identified. Sensitivity experiments configured with varied ratios of VOCs and NOx reduction were conducted to provide a theoretical basis for the development of O_3 mitigation strategies in the Shandong Peninsula.

2. Materials and Methods

2.1. Data Sampling and Quality Assurance/Quality Control

In this study, ambient measurements were conducted at five typical monitoring sites in Shandong Province (locations shown in Figure 1), and the main sources of pollution around the monitoring sites were shown in Figure S1. The monitoring sites included the coastal cities YT, WH, RZ, and DY, and the inland city JN. DY (118.5812° E, 37.4473° N) is located near an oil field exploitation area, with a single source of pollution; there are major petrochemical industry emission sources in the northeast. JN (117.0494° E, 36.6627° N) is located in the center of the city, and is surrounded by a large number of gas stations and construction sites. Sites YT (121.458611° E, 37.46° N), WH (122.1067° E, 37.5069° N), and RZ (119.5192° E, 35.4242° N) are located in the offshore area of the city, where air quality is relatively good.

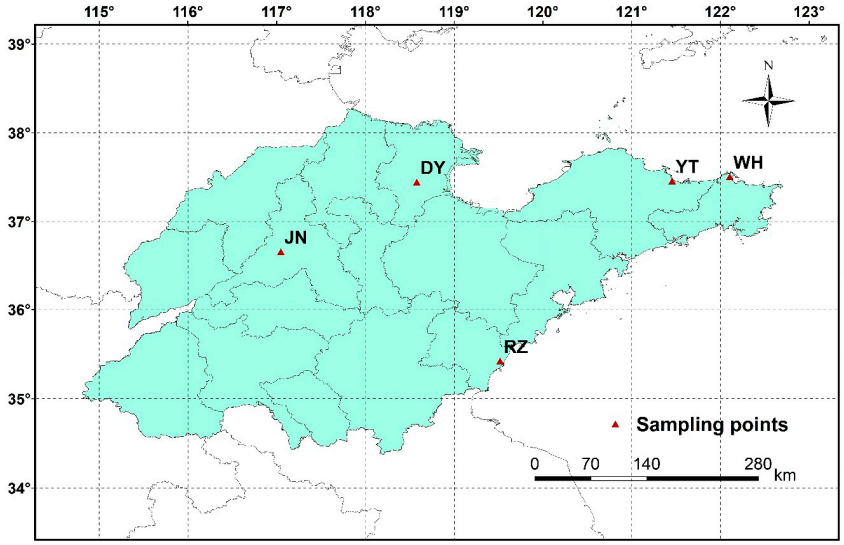

Figure 1. Locations of five monitoring sites (Jinan (JN), Dongying (DY), Rizhao (RZ), Yantai (YT), and Weihai (WH)) across the NCP region.

The VOC data were obtained from the GC955-611 (Hangzhou Juguang Technology Co., Ltd., Hangzhou, China) high boiling point O_3 precursor analyzer online monitoring equipment, which mainly consists of a photo ionization detector and flame ionization detector, a pre-concentration tube, a pre-separation column, an analytical column, a ten-pass valve, and a built-in computer PC, etc. The instrument is loaded with high-purity nitrogen gas and injected at 50 °C without a shunt, and the monitored VOCs included 96 VOC monomers, including 29 alkanes, 11 alkenes, 16 aromatic hydrocarbons, 1 alkyne, 30 halogenated hydrocarbons, and 9 OVOCs. The specific component names are shown in Table S1. The sampling time resolution was 1 h, and 3498 valid samples were obtained over 24 h of continuous monitoring. The online monitor was calibrated every 10 d during the sampling period. The meteorological data were collected simultaneously from the ambient air automatic online monitoring sites with a time resolution of 1 h.

The quality assurance and quality control (QA/QC) of the monitored data is carried out according to the guideline entitled "Specifications and Test Procedures for Ambient Air Quality Continuous Monitoring System with Gas Chromatography for Volatile Organic Compounds" (HJ 1010-2018). The method detection limits (MDLs) of components are 0.01 ppb. The concentration of the blank sample is less than 0.01 ppb. The standard gas was prepared with a volume fraction gradient of 0.5 ppb, 2 ppb, 4 ppb, 6 ppb, 8 ppb, and 10 ppb, and the correlation coefficient of the calibration result should be more than 0.98.

2.2. Ozone Formation Potential

The OFP indicates the potential contribution of individual VOC species to O_3 production, which is an indicator parameter that integrates the reactivity of VOC species to O_3 formation. It can be calculated based on the MIR method [16], and the MIR of VOC species was updated by a previous study [17]. In this study, the OFP of individual VOC species was calculated as follows:

$$C_j^{\mathrm{MIR}} = \mathrm{MIR} \times C_j, \quad (1)$$

$$\mathrm{OFP}_{\mathrm{MIR}} = \sum C_j^{\mathrm{MIR}}, \quad (2)$$

where C_j^{MIR} denotes the maximum O_3 concentration that can be produced by VOC species j, MIR denotes the maximum incremental reactivity of VOC species j, Cj denotes the measured concentration of VOC species j ($\mu g/m^3$), and $\mathrm{OFP}_{\mathrm{MIR}}$ denotes the sum of the maximum O_3 concentration that can be produced by VOC species.

2.3. Weather Research and Forecasting Model

In this study, the Weather Research and Forecasting (WRF) v3.9.1 model was used to simulate meteorological fields from 6 to 22 June 2021 over the NCP region. The initial and boundary conditions of the WRF model were obtained from reanalysis datasets of the National Center for Atmospheric Research (NCAR) with a temporal resolution of 6 h and a spatial resolution of 1° × 1° (https://rda.ucar.edu/datasets/ds083.2/, accessed on 20 October 2022). The vertical resolution of the WRF model was 34 layers. In order to reduce the ambiguity around the initial conditions, the first three days were regarded as the spin-up, which was not included in the analysis. The more detailed options relating to WRF are detailed in Wang et al. [18].

2.4. Observation-Based Model

The Master Chemical Mechanism (MCM, v3.3, http://mcm.leeds.ac.uk/MCM/, accessed on 1 March 2023) model is one of the most important models for investigating atmospheric chemical mechanisms, including 17,000 atmospheric chemical reaction processes of 143 VOCs. Moreover, it is widely used for atmospheric O_3 production mechanisms and VOC sensitive species screening [19–21].

The in situ O_3 production and loss rates were calculated as follows [22,23]: In the troposphere, O_3 production is formed by the reactions of HO_2 + NO and RO_2 + NO. In contrast, O_3 destruction reactions include O_3 photolysis and reactions with VOCs, OH, HO_2, and the reaction of OH + NO_2, RO_2 + NO_2, and VOCs + NO_3. The net O_3 production is defined as the difference between $P(O_3)$ and $L(O_3)$.

$$P(O_3) = k_1[HO_2\cdot][NO] + \sum k_2[RO_2\cdot][NO], \quad (3)$$

$$L(O_3) = k_3\left[O^1(D)\right][\cdot OH] + k_4[\cdot OH][O_3] + k_5[HO_2\cdot][O_3] + k_6[\cdot OH][NO_2] + k_7[RO_2\cdot][NO_2] + 2\sum(k_{8i}[VOC_i][NO_3\cdot]) + \sum(k_{9i}[VOC_i][O_3]), \quad (4)$$

$$NETP(O_3) = P(O_3) - L(O_3) \quad (5)$$

where $P(O_3)$ denotes the O_3 production rate (ppbv/h), $L(O_3)$ represents the O_3 destruction rate (ppbv/h), and k denotes the photochemical reaction rate of the reaction.

The specific model settings of MCM in this study are as follows: During the model simulation, the input data included O_3, VOCs, NOx, and meteorological parameters (Relative humidity, atmospheric pressure, and temperature) with a resolution of 1 h. A special case of a day with high O_3 concentration and complete observation data of the corresponding precursors was selected for model calculation. In this study, the O_3 production and destruction cycle of the high O_3 day was simulated. The model started at 00:00 BST. To ensure the stability of the whole simulation, it was necessary to run it 5 days in advance to obtain the stable concentrations of other atmospheric active species without observations.

In this study, the MCM model simulations were conducted to calculate the daily RIR during O_3 episodes to diagnose O_3 production mechanism. In addition, sensitivity experiments with emission reductions were conducted to probe the RIR changes in response to the reduction of the O_3 precursor. The calculation equation is as follows [19]:

$$RIR(X) = \frac{\Delta P(O_3)(X)/P(O_3)(X)}{\Delta(X)/X}, \quad (6)$$

where $\Delta P(O_3)$ denotes O_3 production rate variations and $\Delta(X)$ denotes the concentration variations of precursor X (VOCs, NO, NO_2).

3. Results

3.1. Temporal Pattern of VOCs

As shown in Figure 2, the concentrations of VOCs in the inland city JN in summer and winter were 27.10 ± 16.44 and 39.90 ± 38.52 ppbv, respectively, which were higher

than the coastal cities (RZ, YT, and WH), while VOC concentrations in the coastal city DY (36.01 ± 23.76 and 96.11 ± 78.84 ppbv) were higher than those of inland cities. Additionally, VOC concentrations in coastal and inland cities in winter were higher than those in summer. Comparing different groups of VOCs, alkanes contribute the most in each city. The maximum concentration of alkanes was 67.99 ± 66.09 ppbv in DN in winter. C_2–C_4 alkanes mainly originate from the use and volatilization of NG/LPG [24], indicating that volatile chemicals from oil fields in DN exerted considerable influence on VOCs. Compared with summer (14–28%), the percentage of OVOCs was significantly lower in winter (3–11%), which is consistent with the findings of other regions [25]. It was found that photochemical reactions make an important contribution to the production of carbonyls [26], indicating that the photochemical reaction rate is lower in winter than in summer due to reduced solar radiation and lower temperature. It is worth noting that both average temperature (28.53 °C) and solar radiation (12.23 W/m^2) in summer is much higher than wintertime (7.30 °C of average temperature and solar radiation as low as 3.95 W/m^2) in JN throughout the sampling period, which, therefore, results in lower OVOC concentrations in winter than in summer.

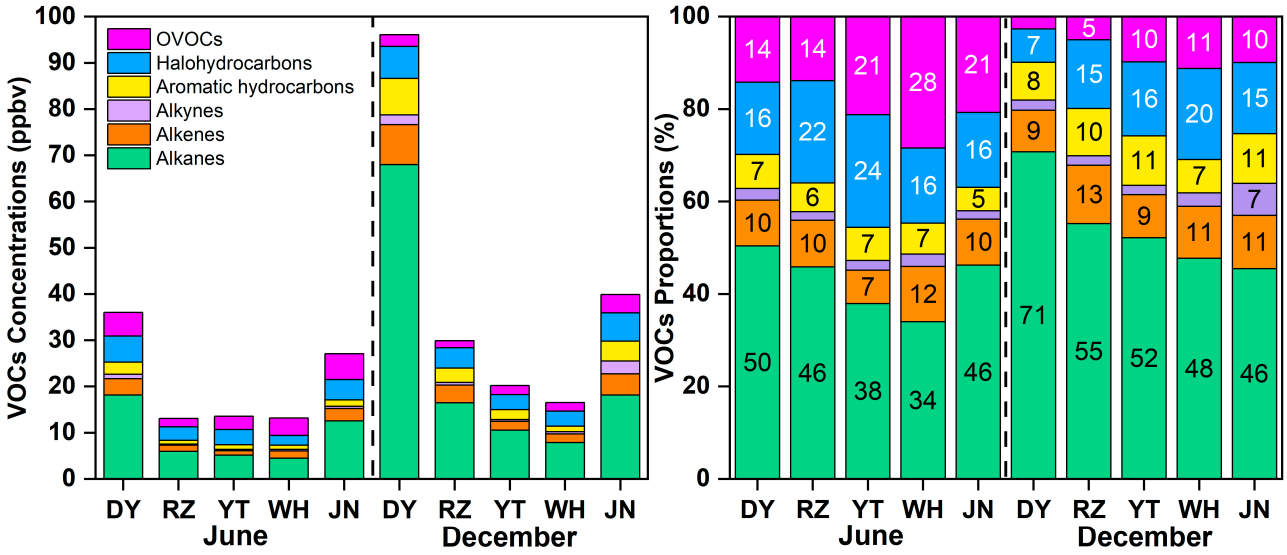

Figure 2. Seasonal distribution of VOC concentrations and proportions in Jinan (JN), Dongying (DY), Rizhao (RZ), Yantai (YT), and Weihai (WH).

Figure 3 shows the diurnal variations of VOC concentrations in coastal and inland cities during June and December 2021. The concentrations of alkanes, alkenes, alkynes, aromatic hydrocarbons, and halohydrocarbons exhibited a decreasing trend during the daytime and an accumulating trend during the nighttime. In contrast, OVOC concentrations showed an opposite diurnal variation. During the daytime, the atmospheric oxidation capacity increases with increasing temperature and solar radiation, which facilitates photochemical reactions that produce OVOCs while enhancing the consumption of other groups of VOCs [11]. At night, the decrease in planetary boundary layer height caused the accumulation of VOC concentrations. Further, it is noteworthy that the diurnal variation for most groups of VOC concentration exhibits double-peak patterns (e.g., at 6:00–8:00 and 19:00–21:00). Compared to inland cities, the peaks of VOCs in the coastal city occurred about a hour earlier. In winter, the daily variation of the same group of VOCs is similar, but its peaks occur about two hours later than those in summer. This pattern has also been observed in other areas [27]. This phenomenon is influenced by local traffic emissions and planetary boundary layer height changes. The planetary boundary layer state is influenced by the temperature and humidity conditions [28]. Stable boundary layers can develop at nighttime, particularly in winter, which causes pollutants to accumulate [29]. This is possibly due to the fact that the convective boundary layer tends to appear earlier in coastal

areas than inland and later in winter than in summer. The concentrations of alkenes and alkynes in coastal areas during summer showed similar diurnal variations, showing several concentration peaks during the daytime (e.g., at 8:00, 10:00, 13:00, and 16:00). This pattern indicates that alkenes and alkynes might originate from the same sources.

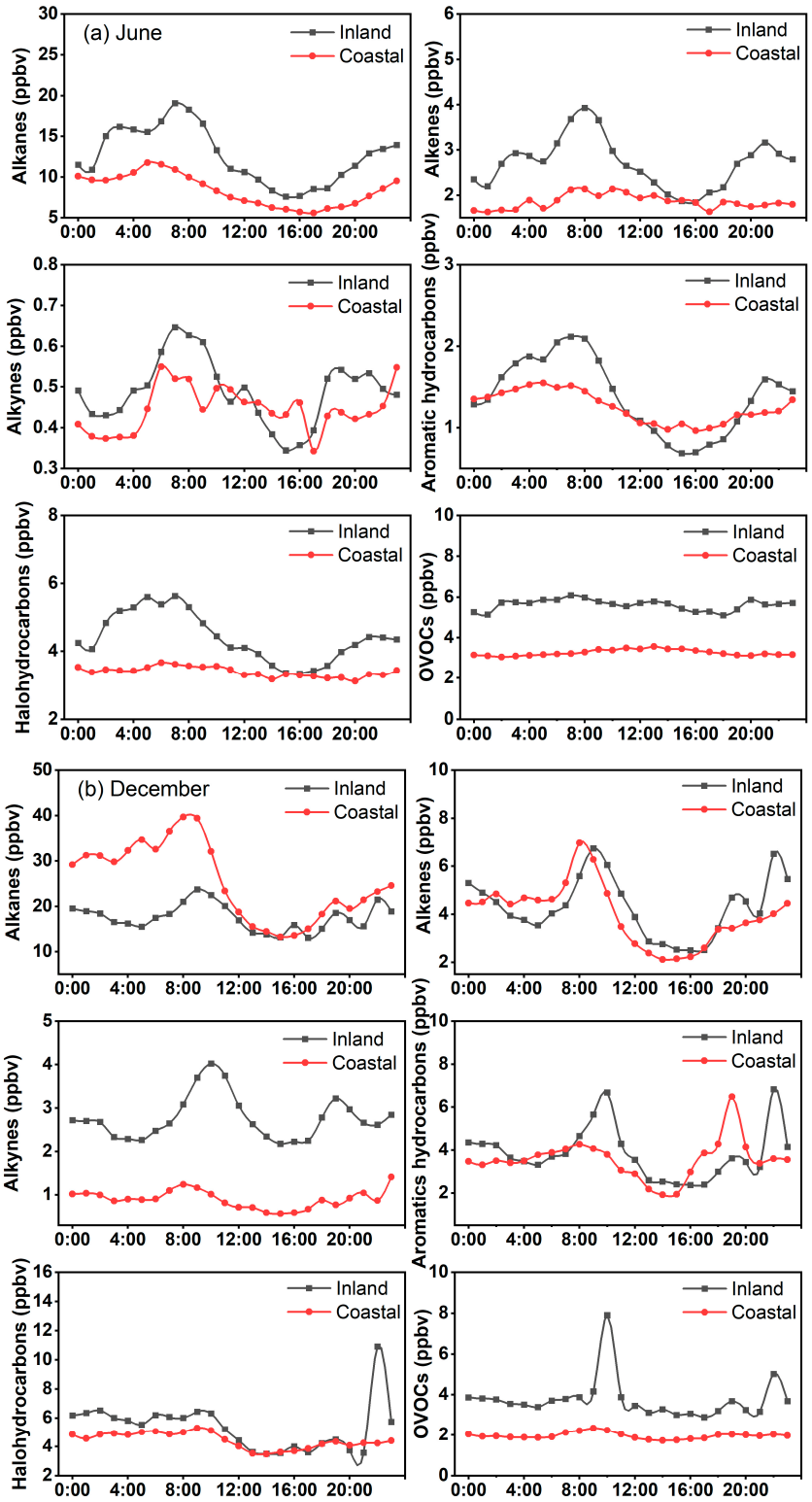

Figure 3. Diurnal variation of VOC concentrations in coastal cities (Dongying (DY), Rizhao (RZ), Yantai (YT), and Weihai (WH)) and an inland city (Jinan (JN)) in June and December.

The concentrations of the top 10 VOC species in coastal and inland cities are shown in Figure 4. Alkanes were the most abundant group in the top 10 VOCs in coastal and inland cities. In contrast to other cities, n-pentane (1.15–3.91 ppbv) and propylene (1.04–1.91 ppbv) are found exclusively in DY. It has been reported that n-pentane and propylene are the major VOC emission components in oil refineries [30]. This revealed that the VOC concentration in DY is predominantly influenced by the local oil field extraction. The components with high concentrations of VOCs in RZ are propane (1.47–4.89 ppbv), ethane (1.66–3.97 ppbv), and n-butane (0.93–3.23 ppbv). Propane, ethane, and acetone were the top three concentrations of VOCs in WH, YT, and JN.

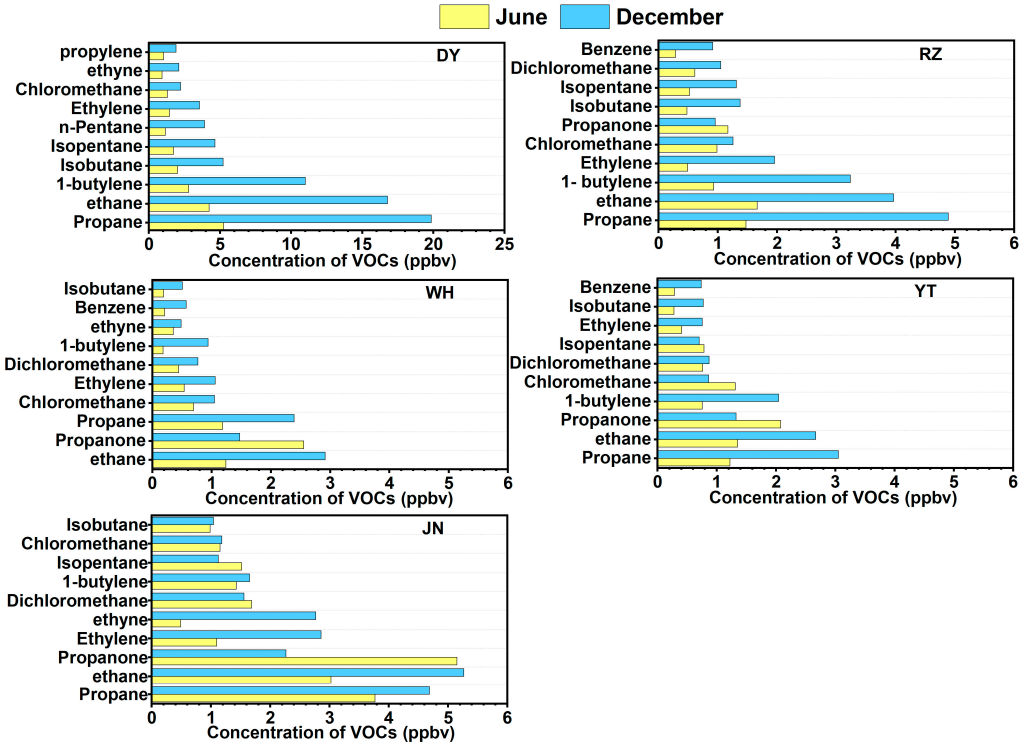

Figure 4. Seasonal distribution of the top 10 VOC species concentrations in Jinan (JN), Dongying (DY), Rizhao (RZ), Yantai (YT), and Weihai (WH) in June and December.

The concentrations of many species are substantially higher in winter than in summer. Conversely, the concentration of acetone is higher in summer than in winter, which is likely due to the effects of emission enhancement from vegetation and the production by oxidation of biogenic hydrocarbons in summer [31]. However, isopentane concentrations in JN and YT were slightly higher in summer than in winter. Isopentane was the main component of the evaporative emissions of motor vehicles [32], with higher temperatures in summer increasing the evaporative emissions of isopentane from motor vehicles. This demonstrates that VOCs in JN and YT are affected by motor vehicle emissions. Additionally, the concentration of dichloromethane in JN and chloromethane in YT is slightly higher in summer than in winter. Dichloromethane and chloromethane were substantial in the chemical industry [33], especially in chlorinated chemical plants [34]. Their concentrations vary in relation to the intensity of urban chemical industry emissions. In conclusion, the major species differences of VOCs between coastal and inland cities are not significant, which is mainly influenced by indigenous emission sources.

3.2. Chemical Reactivity of VOCs

As important precursors of O_3, it is necessary to study the chemical reactivity of VOCs and analyze their effects on O_3 production. The contributions of different groups of VOCs

to OFP_{MIR} among different cities during summer and winter are shown in Figure 5. Table 1 presents the seasonal variation of the top ten VOC species contributing to OFP_{MIR}.

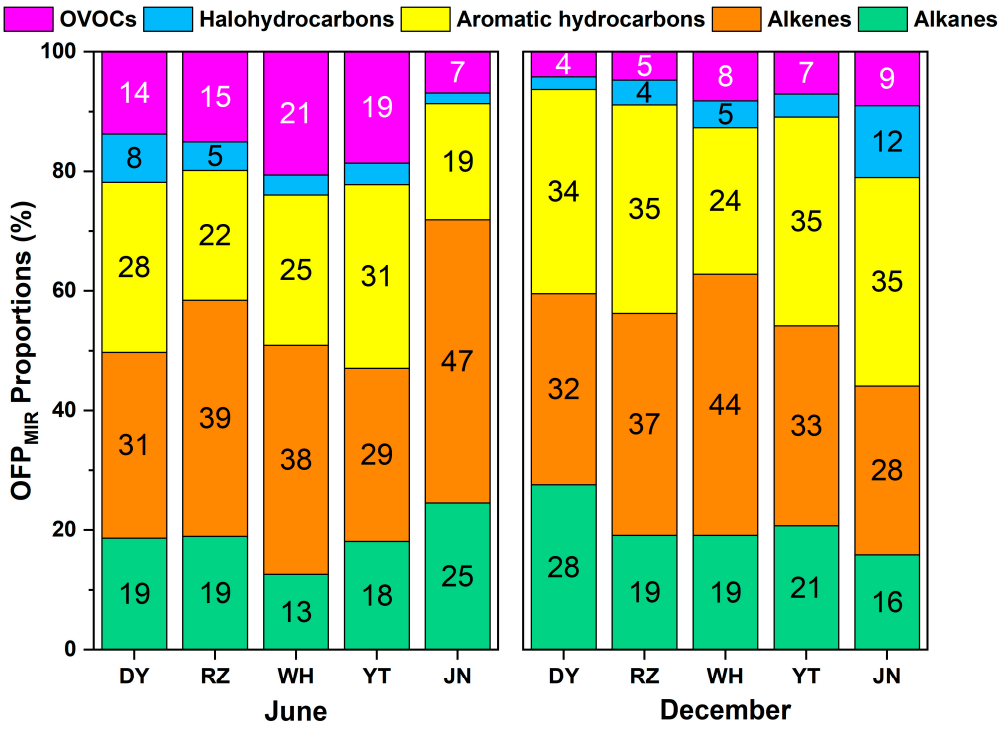

Figure 5. OFP_{MIR} proportions for different types of VOCs in Jinan (JN), Dongying (DY), Rizhao (RZ), Yantai (YT), and Weihai (WH) in June and December.

As shown in Figure 5, the contribution of aromatic hydrocarbons and alkenes to OFP_{MIR} was significant among different cities. This result was also found in other inland [35] and coastal [36] regions. In DY and JN, alkenes were shown to have made the largest contribution (31% and 47%) to O_3 formation in summer, and the contribution of aromatic hydrocarbons in winter increased with 34% and 35%, respectively. RZ and WH have the highest contribution of alkenes in both summer and winter, with 39% and 38% in summer and 37% and 44% in winter. Aromatic hydrocarbons accounted for 31% and 35% of OFP_{MIR} in YT during winter and summer, respectively. In addition, the contribution of OVOCs to O_3 production was more significant in coastal cities in summer compared to inland cities. The results of the top 10 VOC species contributing to OFP_{MIR} (Table 1) showed that m-Xylene + p-Xylene makes the highest contribution to OFP_{MIR} in coastal cities DY (5.19–15.01%), RZ (7.91–17.23%) and YT (11.63–12.93%). This is attributed to the high reactivity of aromatic hydrocarbon. Prior studies have shown that m-Xylene + p-Xylene was a predominant component in printing industry solvent [37] and aromatic hydrocarbon was the most abundant species in wood furniture coating [38] and the petrochemical industry [39]. Further analysis regarding the dominant anthropogenic for monitoring sites suggests that the petrochemical industry may exert a profound influence on DY, and emissions from gas stations may have significant impacts on RZ, WH, and YT. For JN, construction paint may emerge as the dominant contributor due to intense construction activities. In addition, ethylene (6.23–15.96 ppbv) and methylbenzene (1.58–8.04 ppbv) contribute significantly to O_3 production in both inland and coastal cities. Ethylene (11.80%) and methylbenzene (11.27%) were the most abundant VOCs in exhaust gas from on-road vehicles [40]. This suggests that the contribution of vehicle emissions to O_3 production in NCP should not be neglected. The components with high proportional contributions to O_3 formation in WH were ethylene (6.48–15.96%), propylene (5.41–13.17%) and 1,2,4-trimethylbenzene (0.79–11.58%). In coastal regions, ship exhaust emissions contributed significantly to anthropogenic sources of VOCs, with ethylene and 1,2,4-trimethylbenzene

being the main species emitted [41]. This indicates that ship emissions have a relatively large influence on O_3 formation in WH. As the dominant species of biogenic source [42], isoprene contributes to O_3 production in JN and YT during summer, with contributions reaching 6.71% and 5.21%, respectively.

Table 1. Top ten species of VOCs in June and December with their OFP_{MIR} proportions (%) in Jinan (JN), Dongying (DY), Rizhao (RZ), Yantai (YT), and Weihai (WH).

DY	June	December	Variation (%)	RZ	June	December	Variation (%)
m-Xylene + p-Xylene	5.19	15.01	189.02	m-Xylene + p-Xylene	7.91	17.23	117.88
propylene	9.01	7.73	−14.21	Ethylene	6.85	11.57	68.89
Ethylene	6.50	7.37	13.47	1-butylene	11.05	9.60	−13.12
Butadiene	3.27	8.68	165.25	propylene	4.22	7.95	88.43
1-butylene	3.30	6.04	82.85	1-butylene	3.41	5.06	48.25
methylbenzene	3.70	4.67	26.10	trans-2-butene	7.23	3.32	−54.09
ortho-Xylene	2.72	4.60	68.87	methylbenzene	2.44	5.03	105.92
Isopentane	3.19	4.00	25.33	ortho-xylene	2.22	4.46	100.95
1-butylene	2.05	4.49	119.14	Propionaldehyde	7.04	2.13	−69.70
Propane	2.01	3.53	75.82	cis-2-butene	6.32	2.30	−63.64
WH	June	December	Variation (%)	YT	June	December	Variation (%)
Ethylene	6.48	15.96	146.45	m-Xylene + p-Xylene	12.93	11.63	−10.00
propylene	5.41	13.17	143.24	propylene	5.48	9.72	77.35
1,2,4-trimethylbenzene	11.58	0.79	−93.16	Ethylene	6.23	7.57	21.42
m-Xylene + p-Xylene	5.27	7.27	38.12	1-butylene	1.81	8.69	379.49
1-butylene	4.01	7.39	84.23	methylbenzene	2.69	8.04	198.61
cis-2-butene	6.57	2.45	−62.72	Propionaldehyde	9.74	1.96	−79.86
Propionaldehyde	5.81	2.77	−52.33	1-butylene	3.06	5.43	77.69
trans-2-butene	7.33	0.86	−88.29	ortho-xylene	3.94	4.54	15.44
methylbenzene	1.54	5.23	239.69	Isopentane	4.98	2.93	−41.20
butyraldehyde	4.35	0.69	−84.23	Isoprene	5.21	0.56	−89.32
JN	June	December	Variation (%)				
Ethylene	10.06	12.32	22.40				
m-Xylene + p-Xylene	6.11	10.12	65.57				
methylbenzene	5.23	5.97	14.20				
1-butylene	14.03	1.78	−87.30				
propylene	6.05	5.16	−14.81				
ortho-xylene	2.50	4.17	66.83				
Isopentane	5.76	2.00	−65.19				
Isoprene	6.71	1.50	−77.64				
1-butylene	3.46	1.88	−45.64				
1,2,4-trimethylbenzene	1.01	2.81	176.46				

To investigate the influence of VOCs on O_3 formation intensity, the contribution of VOCs OFP_{MIR} at different O_3 concentration levels was calculated. Figure 6 shows the variation in OFP_{MIR} proportions of the VOC groups with the concentration of O_3. In coastal areas, especially YT, the percentage of OVOC OFP_{MIR} increased greatly as O_3 concentration increased, while this phenomenon was not significant in inland areas. This phenomenon is likely influenced by the atmospheric oxidation capacity, which was found to be positively correlated with O_3 concentration in a previous study [43]. The increasing atmospheric

oxidation capacity promotes the secondary production of OVOCs [44]. As with the increase in O_3 concentration, the OFP_{MIR} proportion of aromatic hydrocarbons decreased in RZ, YT, and JN. In DY and WH, alkenes and aromatic hydrocarbons consistently accounted for high proportions of OFP_{MIR}. In JN and RZ, alkenes contribute the most to O_3 formation, and contributions of both alkenes and alkanes increase with the increase in O_3 concentrations, indicating that O_3 formation in these two cities is mainly influenced by alkenes.

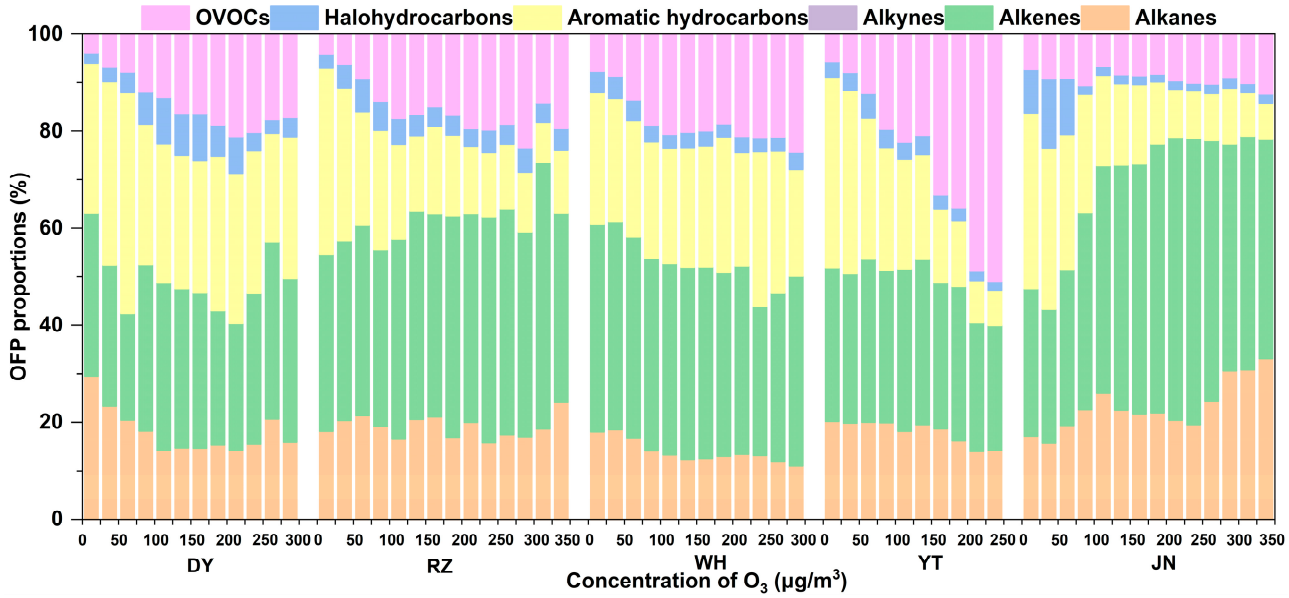

Figure 6. Variation in the proportions of OFP_{MIR} with their O_3 concentration in Jinan (JN), Dongying (DY), Rizhao (RZ), Yantai (YT), and Weihai (WH).

3.3. Model Simulation of O_3 Photochemical Formation

3.3.1. O_3 Formation Based on MCM Modeling

In order to understand the causes of O_3 pollution in different cities from the perspective of chemical reaction pathways, the typical coastal cities DY and RZ and the inland city JN were selected for comparison. O_3 production was simulated based on MCM for these cities on days with high O_3 concentration (DY: 6 June; RZ: 22 June; JN: 8 June). Figure 7 showed the in situ O_3 photochemistry production mechanism on high O_3 pollution days. It was found that the net O_3 production rates in DY, RZ, and JN were 27.87, 10.24, and 10.37 ppbv/h, respectively. This is comparable to the research from another coastal city Xiamen, where the net O_3 production rate was 9.1 ppbv/h [45]. The pathway that contributed most to O_3 production was HO_2 + NO, which had daytime contribution rates of 16.43, 8.98, and 8.19 ppbv/h in DY, RZ, and JN, accounting for 49.29%, 63.66%, and 57.72%, respectively. RO_2 + NO is another pathway with a significant contribution to O_3 production, which is divided into CH_3O_2 + NO with the largest contribution and other RO_2 + NO. The rate of CH_3O_2 + NO was 13.50, 3.63, and 4.67 ppbv/h, accounting for 40.50%, 25.72%, and 32.74%, respectively.

According to the results of the O_3 production pathway, the O_3 production rate in DY (27.87 ppbv/h) is significantly higher than that in the coastal city RZ (10.24 ppbv/h) and the inland city JN (10.37 ppbv/h). The O_3 production pathways in RZ and JN are dominated by HO_2 + NO, while the RO_2 + NO contributes the most to O_3 production in DY. This is mainly caused by the large contribution of the CH_3O_2 + NO (40.50%). CH_3O_2 is the dominant species of RO_2, and it was found that CH_3O_2 accounts for 83% of RO_2. CH_3O_2 is mainly derived from CH_4($OH + CH_4 \rightarrow CH_3O_2$), and CH_3O_2 can react with NO to produce HO_2($CH_3O_2 + NO \rightarrow HCHO + HO_2 + NO_2$), which propagates the HO_X radical and further O_3 production [46,47]. Moreover, it has also been shown that oil extraction is the principal source sector of CH_4. Therefore, it is speculated that the emissions from the

oilfield promote the enrichment of CH_4, which further promotes the reaction of CH_3O_2 with NO, resulting in a higher rate of in situ O_3 production in DY.

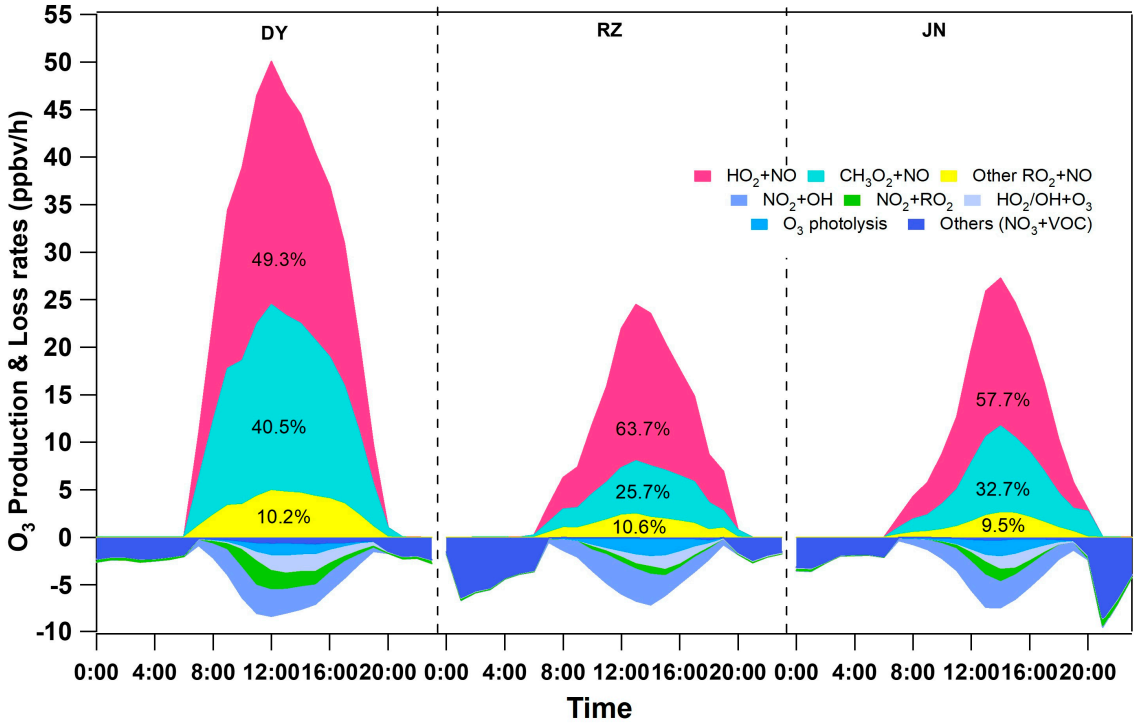

Figure 7. O_3 production and destruction pathways in Dongying (DY), Rizhao (RZ), and Jinan (JN) on days with high O_3 concentration.

The abovementioned analysis shows that the in situ O_3 production rate is different from the observed O_3 concentration variation. This is because the O_3 concentration variation is affected by a combination of in situ photochemical reactions and physical processes [22,23]. The diurnal variation of the net O_3 production rate ($O_{3\text{-Chem}}$) and regional transport O_3 ($O_{3\text{-Tran}}$) as well as the observed O_3 production change rate ($d(O_3/dt)$) in cities during the O_3 pollution process are shown in Figure 8. The rate of O_3 change was calculated from the derivative of the observed O_3 time series ($O_{3\text{-meas}} = d(O_3)/dt$). The rate of in situ O_3 production ($O_{3\text{-chem}}$) is calculated based on the MCM model. The difference between them is the rate of O_3 change for physical transport ($O_{3\text{-tran}} = O_{3\text{-meas}} - O_{3\text{-chem}}$), which incorporates horizontal regional transport and the role of the atmospheric mixed layer [22,23]. To understand the effect of regional transport on O_3 concentration, the spatial distribution of temperature and wind vectors during the O_3 pollution process in Shandong Province was simulated based on the WRF-Chem model shown in Figure 9.

$O_{3\text{-tran}} > 0$ indicates inward transport and $O_{3\text{-tran}} > 0$ indicates outward transport. The transport contributes more to the O_3 concentration in the morning in RZ (8:00–9:00) and JN (8:00–12:00), which is due to the contribution of residual boundary-layer air [48] to O_3. In DY, O_3 concentrations are mainly influenced by in situ production and there is a clear trend of outward export in the afternoon, combined with Figure 9, which shows that it is mainly influenced by easterly winds originating from the ocean and with high wind speed. RZ was influenced by winds from the northeast with low wind speed, where regional transmission has less influence on O_3 concentrations. JN has a larger O_3 transmission in the afternoon and is influenced by southeast transmission from the inland regions.

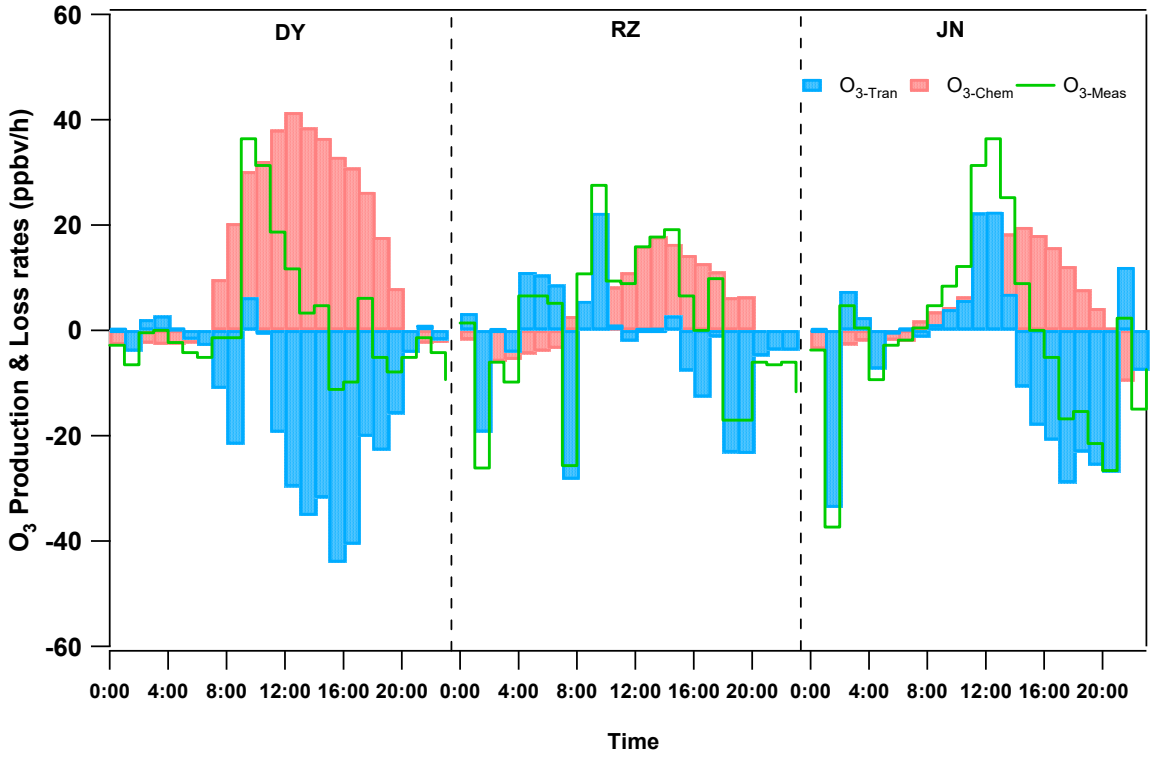

Figure 8. Diurnal variation of the net O_3 production rate ($O_{3\text{-Chem}}$) and regional transport O_3($O_{3\text{-Tran}}$) as well as the observed O_3 production change rate (d(O_3/dt)) in Dongying (DY), Rizhao (RZ), and Jinan (JN) during the O_3 pollution process.

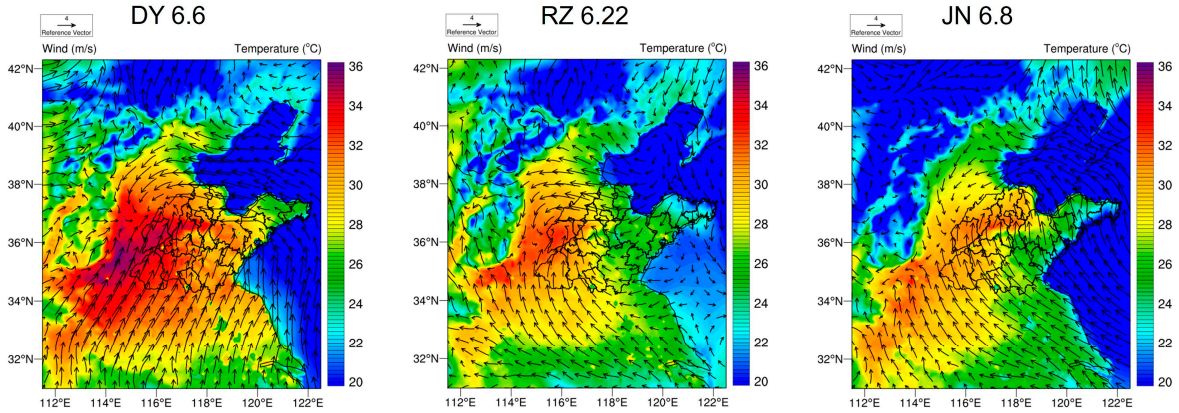

Figure 9. Spatial distribution of temperature and wind vectors of a typical pollution process in Dongying (DY), Rizhao (RZ), and Jinan (JN).

3.3.2. RIR of NOx and VOCs

The simulation of sensitive species abatement scenarios are conducted using model-controlled O_3 production, i.e., the rate of change in O_3 production rates caused by a hypothetical 20% reduction in the concentration of specific O_3 precursors (VOCs and NOx), respectively. The RIR and abatement response are explained by applying the O_3 production mechanism during the observation period [49].

As shown in Figure 10, the formation of high O_3 pollution in DY is limited by VOCs and NOx, while the O_3 production in JN and RZ is mainly the VOC-limited regime. The results of sensitivity experiments undertaken by reducing the concentration of VOCs by 20% showed that the O_3 reduction rates were 15.95%, 20.83%, and 17.19%, respectively. Further sensitivity experiments were conducted by reducing the concentration of different groups

of VOCs by 20%. Additionally, Isoprene was classified as a biogenic alkene (alkene-B) and the other alkenes were categorized as anthropogenic alkenes (alkene-A). Controlling the concentration of aromatic hydrocarbons and alkenes-A could significantly reduce the O_3 formation in DY, and the O_3 reduction rates were calculated to be 3.96% and 3.82%. In JN and RZ, controlling alkenes-A could significantly reduce the O_3 formation with O_3 reduction rates of 9.12% and 12.74%, respectively. In addition, controlling alkane concentrations can also reduce O_3 production, with RIRs of 0.17, 0.11, and 0.23 in DY, RZ, and JN, respectively. Compared to coastal cities, inland city JN O_3 production was more sensitive to alkene-B, with an RIR of 0.16. In contrast, O_3 production was more sensitive to OVOCs, with RIRs of 0.11 and 0.10 in coastal regions DY and RZ, respectively. Therefore, alkenes and aromatic hydrocarbons are the key groups that have a large impact on O_3 production during periods of heavy O_3 pollution. In DY, reducing aromatic hydrocarbons and alkenes can effectively mitigate O_3 pollution, and in JN and RZ, reducing alkene concentrations can reduce O_3 pollution. This conclusion is consistent with the results of the OFP analysis in 3.2 (Figures 5 and 6).

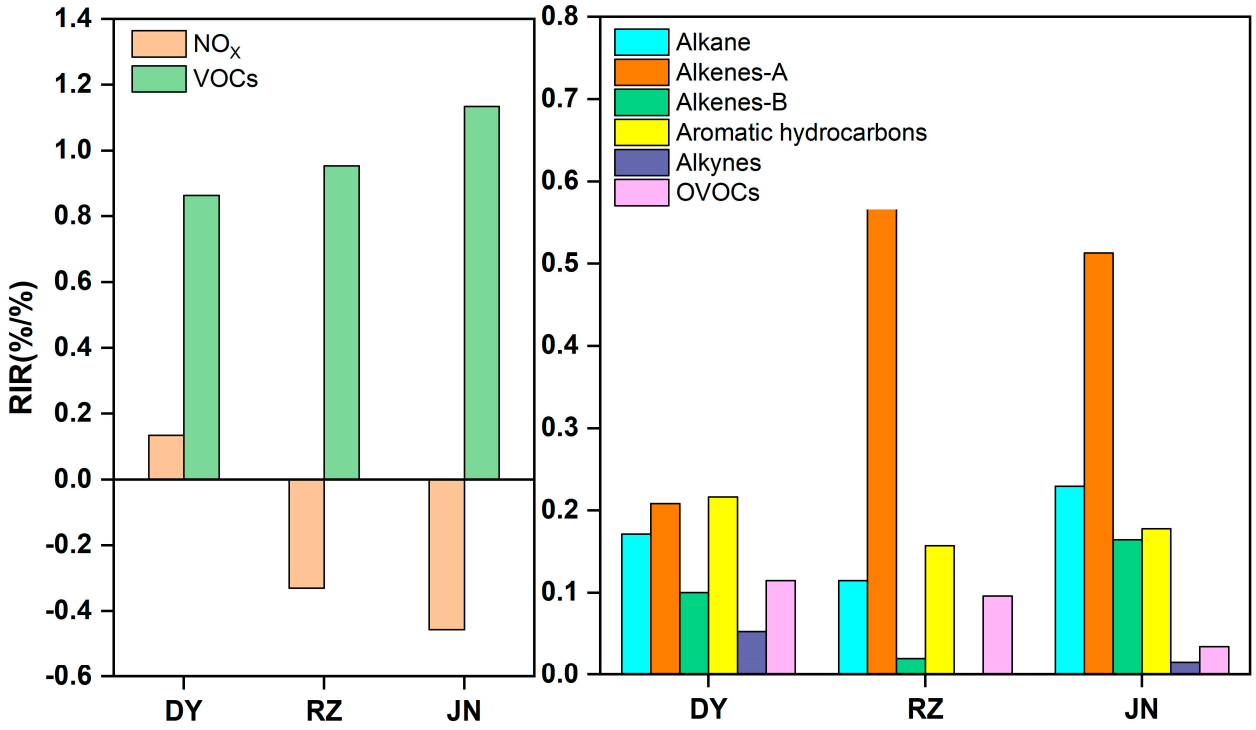

Figure 10. Relative incremental reactivity (RIR) of the major O_3 precursor VOCs and NO_X in Dongying (DY), Rizhao (RZ), and Jinan (JN).

To investigate the effect of individual species on O_3 production, sensitivity experiments were conducted on individual species of the most sensitive VOC species in each city. As shown in Figure 11, in DY, the most sensitive species among aromatic hydrocarbons was m-Xylene + p-Xylene, followed by mesitylene, 1,2,4-trimethylbenzene, and methylbenzene. The species with the highest contribution to O_3 production among alkenes was butene, in JN and RZ. Moreover, trans-2-butene, cis-2-butene, and 1-butylene made a significant contribution to O_3 production in RZ with RIRs of 0.26, 0.23, and 0.05, respectively. It was found that decreasing the concentration of cis-2-butene, 1-butylene, and trans-2-butene led to the greatest change in O_3 production rate at JN, with RIRs of 0.14, 0.95, and 0.07, respectively. This result is consistent with previous studies in Zibo [19], where C_2–C_5 alkenes and C_7–C_9 aromatic hydrocarbons contributed greatly to O_3 production. It was found that aromatic hydrocarbons were the characteristic compounds of architectural coatings and solvents [50], and cis-2-butene, 1-butylene, and trans-2-butene all originate

from vehicle exhaust and liquefied petroleum gas (LPG) [51]; therefore, cities should further implement targeted control of their emissions.

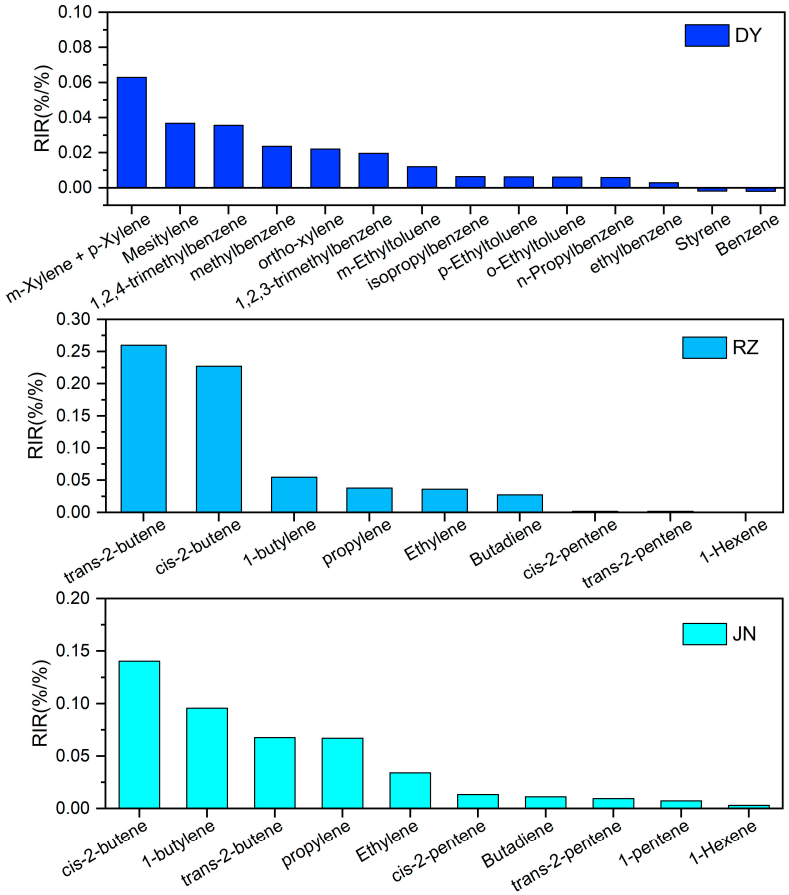

Figure 11. Relative incremental reactivity (RIR) of VOC species in Dongying (DY), Rizhao (RZ), and Jinan (JN).

The results of sensitivity experiments showed that the effect of important precursors of O_3 (NO_X and VOCs) on O_3 production varies in different contexts. O_3 production rate increases with the decrease of NO_X concentrations, and the relationship between O_3 and NO_X is complex. Therefore, this study further simulates the O_3 production rate in the set of assumed NO_X and VOCs with different concentration gradients, i.e., NO_X and VOC concentrations are respectively reduced by 10–80% and increased by 10–40%, then input to the model for simulation. The net O_3 production rates for different abatement scenarios are shown in Figure 12, and the corresponding RIRs are given in Table 2.

Table 2. Relative incremental reactivity (RIR) of different reduction ratios of NO_X and VOCs in Dongying (DY), Rizhao (RZ), and Jinan (JN) (%/%).

Reduction Ratios		140%	130%	120%	110%	90%	80%	70%	60%	50%	40%	30%	20%
NOx	DY	−0.027	−0.004	0.019	0.040	0.151	0.173	0.237	0.300	0.373	0.454	0.566	0.699
	RZ	−0.350	−0.355	−0.364	−0.340	−0.304	−0.301	−0.283	−0.234	−0.181	−0.108	0.014	0.193
	JN	−0.402	−0.413	−0.407	−0.404	−0.424	−0.391	−0.378	−0.339	−0.282	−0.198	−0.052	0.183
VOCs	DY	0.704	0.721	0.749	0.733	0.837	0.867	0.896	0.924	0.955	0.983	1.007	1.019
	RZ	0.920	0.927	0.925	0.928	0.951	0.945	0.943	0.938	0.939	0.934	0.928	0.921
	JN	1.118	1.131	1.133	1.152	1.098	1.121	1.113	1.101	1.089	1.071	1.050	1.025

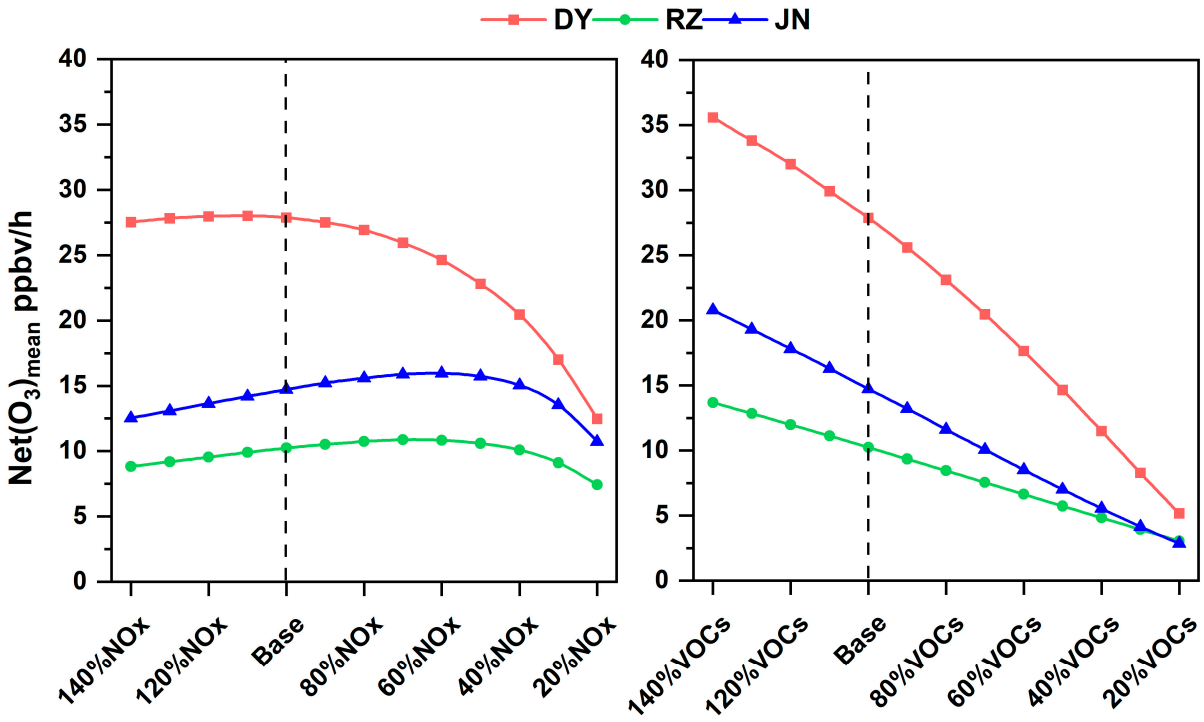

Figure 12. O_3 production rates for different reduction ratios of NO_X and VOCs in Dongying (DY), Rizhao (RZ), and Jinan (JN).

Different concentration gradients of emission reduction revealed that O_3 production in three cities was more sensitive to VOCs compared to NO_X, and reducing VOC concentration can lead to a significant reduction in net O_3 production rate. Based on the slope (Figure 12), it can be concluded that O_3 production in DY is the most sensitive to VOC emission reduction. Further, based on the RIR values in response to the varied reduction ratio (Table 2), it is seen that RIR values increase with the incremental reduction of VOCs in DY, which indicates a higher reduction rate of O_3 production. However, the scenario of 10% abatement of VOC concentration in RZ has the most significant effect on O_3 production, with an RIR of 0.951. In contrast, the response of emission reduction in JN is much more complex. In the context of reducing VOC concentration, when VOC concentration is reduced by 20%, O_3 sensitivity is the highest, and the RIR is 1.12. However, a 10% increase in VOC concentration has a stronger O_3 production response, with an RIR of 1.15. This situation indicates that VOC emission in JN can lead to a significant increase in the O_3 production rate.

The response of the net O_3 production rate to the change of NO_X concentration in each city is not evident, and sensitivity is ranked as follows: DY > JN > RZ. Reducing NO_X concentration in DY can lead to a lower O_3 production rate, and the RIR peaks at 0.699 when the NO_X concentration is multiplied by 20%. The O_3 production rate also decreases when NO_X concentration increases by more than 30%. In RZ and JN, O_3 production rate would decrease only when the NO_X reduction ratio is more than 60% and 70%, respectively. When the NO_X concentration is reduced by 80%, the RIR reaches the maximum value of 1.93 and 1.83, respectively. The phenomenon by means of which increasing NO_X concentration decreases the O_3 production rate indicates that NO_X concentration plays a titration role in O_3 production [52]. The difference in O_3 production rates between cities with respect to NO_X sensitivity in this study, which is postulated to be related to the differences in NO_X concentrations in different cities, deserves further investigation.

To better understand the relationship between NO_X concentration and O_3 production rate, the hourly simulation results of different cities are summarized. Figure 13 shows the distribution of NO_X concentration change and RIR during the daytime (7:00–19:00). The

effect of NO_X concentration on the change of O_3 production rate is expressed by RIR; when RIR is positive, it means that the change of NO_X concentration is positively correlated with the O_3 production rate, and vice versa, it is negatively correlated, and the magnitude of the absolute value of RIR indicates the magnitude of sensitivity. An important phenomenon was also demonstrated, which was a negative RIR in the morning (9:00–11:00) and a positive RIR in the afternoon (15:00–17:00) with greater sensitivity at lower NO_X concentrations. This phenomenon was also found in other studies, where O_3 production in California shifted towards a more NO_X-sensitive scenario in the afternoon [53], indicating that when the NO_X concentration is at a high level in the morning, the effect on the O_3 production rate is negatively correlated, i.e., reducing the NO_X concentration will decrease the titration effect on O_3 production, resulting in elevated ozone concentration. Conversely, greater efficiency of O_3 reduction could be achieved by reducing NO_X when the NO_X concentration is low (less than 20 ppbv in this study) in the afternoon.

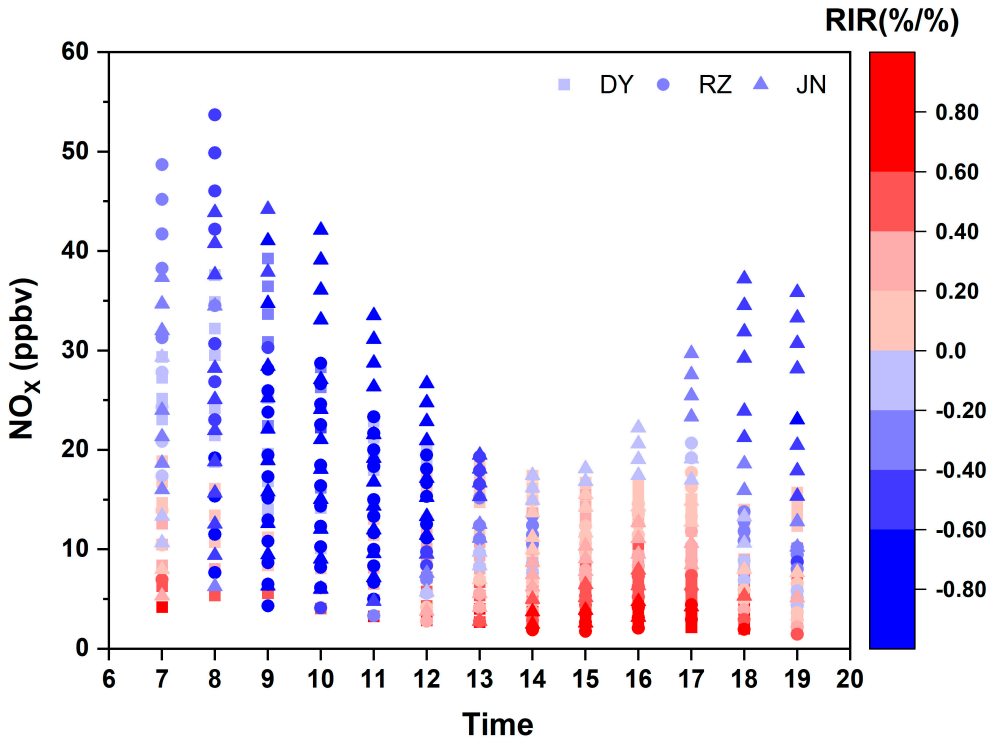

Figure 13. Distribution of NO_X concentration variation and RIR during the daytime (7:00–19:00) in Dongying (DY), Rizhao (RZ), and Jinan (JN).

4. Discussion

In this study, we measured VOCs by GC-MS in five cities over the NCP for two sampling periods (June and December) in 2021. The detailed chemical composition and reactivity of VOCs are investigated and the implications for O_3 formation are examined using the OBM.

Previous studies have investigated VOC components which have a single sampling point location and brief sampling period. In this study, different coastal and inland cities were purposely selected and a large amount of data was comprehensively analyzed. Consistent with the findings of other regions [10,25], alkanes contribute the most to VOCs in NCP; however, the alkanes accounted for 71% of VOCs in DY during winter, which was significantly higher than previous studies (45.88%) [54]. This was caused by the volatile emissions from oil fields in DY. The major species differences of VOCs between coastal and inland cities, which are mainly influenced by indigenous emission sources, are not significant.

It is found that the differences in VOC composition between cities not only affect the O_3 potential but also the main pathways of O_3 production. The O_3 production rate in DY

(27.87 ppbv/h) is significantly higher than that in the coastal city RZ (10.24 ppbv/h) and Xiamen (9.1 ppbv/h) [45]. The O_3 production pathways in RZ and JN are dominated by HO_2 + NO, while RO_2 + NO contributes the most to O_3 production in DY. It is speculated that oil field emissions promote the enrichment of CH_4, which further promotes the reaction of CH_3O_2 with NO [46,47], resulting in a higher rate of in situ O_3 production in DY. Furthermore, our results suggest that the O_3 abatement response sensitivities are impacted by differences in VOCs and NOx concentrations. The response between O_3 and NO_X has a clear daily variation pattern (the sensitivity is greater from 15:00 to 17:00 in the afternoon), which was also found in California [53].

The major limitation of the present study is that, apart from isoprene, we did not measure biogenic VOCs, which contribute greatly to O_3 formation. Moreover, the identification of dominant anthropogenic emission sources in monitoring sites is limited to emission features, and thereby requires quantitative source apportionment from chemical transport models. Therefore, an expanded ambient monitoring network with routine measurements of VOCs (biogenic and anthropogenic) and high-resolution chemical transport modeling are needed to further elucidate the characteristics of VOCs and their effect on O_3 formation.

5. Conclusions

In this study, we characterize the spatial and temporal patterns of VOCs and investigate the O_3 production mechanism on an O_3 pollution day over the NCP region. For the temporal distribution of VOCs, except OVOCs, the concentrations of VOCs are greatly higher in winter than summer and the daily variation shows a pattern of decreasing during the daytime and accumulating during the nighttime, while the seasonal and diurnal variation patterns of OVOC concentrations are the opposite. The peaks of VOC diurnal concentration in the coastal city occurred earlier compared with inland city. Alkanes accounted for the largest proportion of VOCs in cities, particularly in DY, where alkanes contributed 71% of VOCs, which were affected by oil field emissions. The chemical reactivity of VOCs suggests that aromatic hydrocarbons and alkenes contribute most to OFP in NCP. In addition, compared to inland cities, the contribution of OVOCs to O_3 production was more significant in coastal cities during summer.

The in situ O_3 photochemistry production mechanism on high O_3 pollution days showed that net O_3 production rates in DY, RZ, and JN were 27.87, 10.24, and 10.37 ppbv/h. The pathway that contributed most to O_3 production was HO_2 + NO, followed by RO_2 + NO (CH_3O_2 + NO and other RO_2 + NO). The formation of high O_3 pollution in DY in summer was the transitional regime, but it's VOC-limited in JN and RZ. Alkenes and aromatic hydrocarbons are the key groups that have a large impact on O_3 production during periods of heavy O_3 pollution. Reducing aromatic hydrocarbons (m/p-xylene) and alkenes (butene) can effectively mitigate O_3 pollution in NCP.

Different concentration gradients of emission reduction revealed that O_3 production in DY is the most sensitive to VOCs emission reduction. The response of the net O_3 production rate to the change in NO_X concentration is not obvious, and the sensitivity is DY > JN > RZ. The response between O_3 and NO_X is influenced by the NO_X concentration and has a clear daily variation pattern (the sensitivity is greater from 15:00 to 17:00 in the afternoon). The greatest efficiencies in O_3 reduction could be achieved by reducing NO_X when the NO_X concentration is low (less than 20 ppbv in this study).

Supplementary Materials: The following supporting information can be downloaded at: https://www.mdpi.com/article/10.3390/atmos15020213/s1, Figure S1. Main sources of pollution around monitoring sites (Jinan (JN), Dongying (DY), Rizhao (RZ), Yantai (YT) and Weihai (WH)). Table S1. The name of the compound monitored in this study.

Author Contributions: Conceptualization, G.Z.; methodology, Y.S.; software, Q.D.; formal analysis, X.W.; investigation, L.F.; data curation, H.Y. and M.Z.; writing—original draft preparation, S.H.; writing—review and editing, S.L. All authors have read and agreed to the published version of the manuscript.

Funding: This research was funded by Shandong Top Talent Special Foundation of China, grant number 0031504; Shandong Provincial Natural Science Foundation of China, grant number ZR2021MD013 and ZR2020ZD21; Key R&D Program of Shandong Province, China, grant number 2020CXGC011401; and Construction of High-quality Courses in Graduate Education of China, grant number YZKC202214.

Institutional Review Board Statement: Not applicable.

Informed Consent Statement: Not applicable.

Data Availability Statement: Data is contained within the article.

Acknowledgments: We gratefully acknowledge the review provided by four anonymous reviewers.

Conflicts of Interest: The authors declare no conflicts of interest. Saimei Hao are employees of Qingdao Gemini Scientific Co., Ltd. The paper reflects the views of the scientists and not the company.

References

1. Tao, T.; Shi, Y.; Gilbert, K.M.; Liu, X. Spatiotemporal variations of air pollutants based on ground observation and emission sources over 19 Chinese urban agglomerations during 2015–2019. *Sci. Rep.* **2022**, *12*, 2045–2322. [CrossRef]
2. Li, X.; Chen, Q.; Zheng, X.; Li, Y.; Han, M.; Liu, T.; Xiao, J.; Guo, L.; Zeng, W.; Zhang, J.; et al. Effects of ambient ozone concentrations with different averaging times on asthma exacerbations: A meta-analysis. *Sci. Total Environ.* **2019**, *691*, 549–561. [CrossRef] [PubMed]
3. Zhang, Y.; Tian, Q.; Wei, X.; Feng, X.; Ma, P.; Hu, W.; Xin, J.; Ni, C.; Wang, S.; Zheng, C. Temperature modulation of adverse consequences of ozone exposure on cardiovascular mortality: A study of multiple cities in China. *Atmos. Environ.* **2022**, *288*, 119272. [CrossRef]
4. Jurán, S.; Edwards-Jonášová, M.; Cudlín, P.; Zapletal, M.; Šigut, L.; Grace, J.; Urban, O. Prediction of ozone effects on net ecosystem production of Norway spruce forest. *iForest-Biogeosci. For.* **2018**, *11*, 743–750. [CrossRef]
5. Juráň, S.; Grace, J.; Urban, O. Temporal Changes in Ozone Concentrations and Their Impact on Vegetation. *Atmosphere* **2021**, *12*, 82. [CrossRef]
6. Wei, W.; Wang, X.; Wang, X.; Li, R.; Zhou, C.; Cheng, S. Attenuated sensitivity of ozone to precursors in Beijing–Tianjin–Hebei region with the continuous NOx reduction within 2014–2018. *Sci. Total Environ.* **2022**, *813*, 152589. [CrossRef]
7. Sha, Q.; Zhu, M.; Huang, H.; Wang, Y.; Huang, Z.; Zhang, X.; Tang, M.; Lu, M.; Chen, C.; Shi, B.; et al. A newly integrated dataset of volatile organic compounds (VOCs) source profiles and implications for the future development of VOCs profiles in China. *Sci. Total Environ.* **2021**, *793*, 148348. [CrossRef]
8. Feng, Y.; An, J.; Tang, G.; Zhang, Y.; Wang, J.; Lv, H. Characteristics and Sources of Volatile Organic Compounds in the Nanjing Industrial Area. *Atmosphere* **2022**, *13*, 1136. [CrossRef]
9. Sun, J.; Shen, Z.; Wang, R.; Li, G.; Zhang, Y.; Zhang, B.; He, K.; Tang, Z.; Xu, H.; Qu, L.; et al. A comprehensive study on ozone pollution in a megacity in North China Plain during summertime: Observations, source attributions and ozone sensitivity. *Environ. Int.* **2021**, *146*, 106279. [CrossRef]
10. Wang, Z.; Wang, H.; Zhang, L.; Guo, J.; Li, Z.; Wu, K.; Zhu, G.; Hou, D.; Su, H.; Sun, Z.; et al. Characteristics of volatile organic compounds (VOCs) based on multisite observations in Hebei province in the warm season in 2019. *Atmos. Environ.* **2021**, *256*, 118435. [CrossRef]
11. Ji, X.; Xu, K.; Liao, D.; Chen, G.; Liu, T.; Hong, Y.; Dong, S.; Choi, S.; Chen, J. Spatial-temporal Characteristics and Source Apportionment of Ambient VOCs in Southeast Mountain Area of China. *Aerosol Air Qual. Res.* **2022**, *22*, 220016. [CrossRef]
12. Liu, Y.; Wang, H.; Jing, S.; Gao, Y.; Peng, Y.; Lou, S.; Cheng, T.; Tao, S.; Li, L.; Li, Y.; et al. Characteristics and sources of volatile organic compounds (VOCs) in Shanghai during summer: Implications of regional transport. *Atmos. Environ.* **2019**, *215*, 116902. [CrossRef]
13. Wei, J.; Li, Z.; Li, K.; Dickerson, R.R.; Pinker, R.T.; Wang, J.; Liu, X.; Sun, L.; Xue, W.; Cribb, M. Full-coverage mapping and spatiotemporal variations of ground-level ozone (O_3) pollution from 2013 to 2020 across China. Remote Sens. *Environ.* **2022**, *270*, 112775.
14. Zhang, J.; Wang, C.; Qu, K.; Ding, J.; Shang, Y.; Liu, H.; Wei, M. Characteristics of Ozone Pollution, Regional Distribution and Causes during 2014–2018 in Shandong Province, East China. *Atmosphere* **2019**, *10*, 501. [CrossRef]
15. Sun, J.; Duan, S.; Wang, B.; Sun, L.; Zhu, C.; Fan, G.; Sun, X.; Xia, Z.; Lv, B.; Yang, J.; et al. Long-Term Variations of Meteorological and Precursor Influences on Ground Ozone Concentrations in Jinan, North China Plain, from 2010 to 2020. *Atmosphere* **2022**, *13*, 994. [CrossRef]
16. Carter, W.P.L. Computer modeling of environmental chamber measurements of maximum incremental reactivities of volatile organic compounds. *Atmos. Environ.* **1995**, *29*, 2513–2527. [CrossRef]
17. Carter, W.P.L. Updated maximun incremental reactivity scale and hydrocarbon bin reactivities for regulatory applications. *Calif. Air Resour. Board Contract* **2009**, *339*, 2009.
18. Wang, S.; Tsona, N.T.; Du, L. Effect of NOx on secondary organic aerosol formation from the photochemical transformation of allyl acetate. *Atmos. Environ.* **2021**, *255*, 118426. [CrossRef]

19. Lin, H.; Wang, M.; Duan, Y.; Fu, Q.; Ji, W.; Cui, H.; Jin, D.; Lin, Y.; Hu, K. O_3 Sensitivity and Contributions of Different NMHC Sources in O_3 Formation at Urban and Suburban Sites in Shanghai. *Atmosphere* **2020**, *11*, 295. [CrossRef]
20. Wang, M.; Hu, K.; Chen, W.; Shen, X.; Li, W.; Lu, X. Ambient Non-Methane Hydrocarbons (NMHCs) Measurements in Baoding, China: Sources and Roles in Ozone Formation. *Atmosphere* **2020**, *11*, 1205. [CrossRef]
21. Zhang, K.; Liu, Z.; Zhang, X.; Li, Q.; Jensen, A.; Tan, W.; Huang, L.; Wang, Y.; de Gouw, J.; Li, L. Insights into the significant increase in ozone during COVID-19 in a typical urban city of China. *Atmos. Chem. Phys.* **2022**, *22*, 4853–4866. [CrossRef]
22. Li, K.; Wang, X.; Li, L.; Wang, J.; Liu, Y.; Cheng, X.; Xu, B.; Wang, X.; Yan, P.; Li, S.; et al. Large variability of O_3-precursor relationship during severe ozone polluted period in an industry-driven cluster city (Zibo) of North China Plain. *J. Clean. Prod.* **2021**, *316*, 128252. [CrossRef]
23. Xue, L.K.; Wang, T.; Gao, J.; Ding, A.J.; Zhou, X.H.; Blake, D.R.; Wang, X.F.; Saunders, S.M.; Fan, S.J.; Zuo, H.C.; et al. Ground-level ozone in four Chinese cities: Precursors, regional transport and heterogeneous processes. *Atmos. Chem. Phys.* **2014**, *14*, 13175–13188. [CrossRef]
24. Hui, L.; Liu, X.; Tan, Q.; Feng, M.; An, J.; Qu, Y.; Zhang, Y.; Deng, Y.; Zhai, R.; Wang, Z. VOC characteristics, chemical reactivity and sources in urban Wuhan, central China. *Atmos. Environ.* **2020**, *224*, 117340. [CrossRef]
25. Wang, F.; Du, W.; Lv, S.; Ding, Z.; Wang, G. Spatial and Temporal Distributions and Sources of Anthropogenic NMVOCs in the Atmosphere of China: A Review. *Adv. Atmos. Sci.* **2021**, *38*, 1085–1100. [CrossRef] [PubMed]
26. Chen, T.; Zheng, P.; Zhang, Y.; Dong, C.; Han, G.; Li, H.; Yang, X.; Liu, Y.; Sun, J.; Li, H.; et al. Characteristics and formation mechanisms of atmospheric carbonyls in an oilfield region of northern China. *Atmos. Environ.* **2022**, *274*, 118958. [CrossRef]
27. Chen, P.; Zhao, X.; Wang, O.; Shao, M.; Xiao, X.; Wang, S.; Wang, Q.G. Characteristics of VOCs and their Potentials for O3 and SOA Formation in a Medium-sized City in Eastern China. *Aerosol Air Qual. Res.* **2022**, *22*, 210239.
28. Helbig, M.; Gerken, T.; Beamesderfer, E.R.; Baldocchi, D.D.; Banerjee, T.; Biraud, S.C.; Brown, W.O.J.; Brunsell, N.A.; Burakowski, E.A.; Burns, S.P.; et al. Integrating continuous atmospheric boundary layer and tower-based flux measurements to advance understanding of land-atmosphere interactions. *Agr. For. Meteorol.* **2021**, *307*, 108509. [CrossRef]
29. Yin, J.; Gao, C.Y.; Hong, J.; Gao, Z.; Li, Y.; Li, X.; Fan, S.; Zhu, B. Surface Meteorological Conditions and Boundary Layer Height Variations During an Air Pollution Episode in Nanjing, China. *J. Geophys. Res. Atmos.* **2019**, *124*, 3350–3364. [CrossRef]
30. Wei, W.; Lv, Z.; Yang, G.; Cheng, S.; Li, Y.; Wang, L. VOCs emission rate estimate for complicated industrial area source using an inverse-dispersion calculation method: A case study on a petroleum refinery in Northern China. *Environ. Pollut.* **2016**, *218*, 681–688. [CrossRef]
31. Guo, H.; Ling, Z.H.; Cheung, K.; Wang, D.W.; Simpson, I.J.; Blake, D.R. Acetone in the atmosphere of Hong Kong: Abundance, sources and photochemical precursors. *Atmos. Environ.* **2013**, *65*, 80–88. [CrossRef]
32. Yue, T.T.; Yue, X.; Chai, F.H.; Hu, J.N.; Lai, Y.T.; He, L.Q.; Zhu, R.C. Characteristics of volatile organic compounds (VOCs) from the evaporative emissions of modern passenger cars. *Atmos. Environ.* **2017**, *151*, 62–69. [CrossRef]
33. Cheng, N.; Jing, D.; Zhang, C.; Chen, Z.; Li, W.; Li, S.; Wang, Q. Process-based VOCs source profiles and contributions to ozone formation and carcinogenic risk in a typical chemical synthesis pharmaceutical industry in China. *Sci. Total Environ.* **2021**, *752*, 141899. [CrossRef] [PubMed]
34. Mo, Z.; Shao, M.; Lu, S.; Qu, H.; Zhou, M.; Sun, J.; Gou, B. Process-specific emission characteristics of volatile organic compounds (VOCs) from petrochemical facilities in the Yangtze River Delta, China. *Sci. Total Environ.* **2015**, *533*, 422–431. [CrossRef] [PubMed]
35. Sun, J.; Shen, Z.; Zhang, Y.; Zhang, Z.; Zhang, Q.; Zhang, T.; Niu, X.; Huang, Y.; Cui, L.; Xu, H.; et al. Urban VOC profiles, possible sources, and its role in ozone formation for a summer campaign over Xi'an, China. *Environ. Sci. Pollut. Res.* **2019**, *26*, 27769–27782. [CrossRef]
36. Ou, J.; Zheng, J.; Li, R.; Huang, X.; Zhong, Z.; Zhong, L.; Lin, H. Speciated OVOC and VOC emission inventories and their implications for reactivity-based ozone control strategy in the Pearl River Delta region, China. *Sci. Total Environ.* **2015**, *530*, 393–402. [CrossRef]
37. Lin, C.; Liou, N.; Sun, E. Applications of open-path Fourier transform infrared for identification of volatile organic compound pollution sources and characterization of source emission behaviors. *J. Air Waste Manag. Assoc.* **2008**, *58*, 821–828. [CrossRef]
38. Wu, K.Y.; Duan, M.; Zhou, J.B.; Zhou, Z.H.; Tan, Q.W.; Song, D.L.; Lu, C.W.; Deng, Y. Sources Profiles of Anthropogenic Volatile Organic Compounds from Typical Solvent Used in Chengdu, China. *J. Environ. Eng.* **2020**, *146*, 733–9372. [CrossRef]
39. Wu, C.; Wu, T.; Hashmonay, R.A.; Chang, S.; Wu, Y.; Chao, C.; Hsu, C.; Chase, M.J.; Kagann, R.H. Measurement of fugitive volatile organic compound emissions from a petrochemical tank farm using open-path Fourier transform infrared spectrometry. *Atmos. Environ.* **2014**, *82*, 335–342. [CrossRef]
40. Wang, J.; Jin, L.; Gao, J.; Shi, J.; Zhao, Y.; Liu, S.; Jin, T.; Bai, Z.; Wu, C. Investigation of speciated VOC in gasoline vehicular exhaust under ECE and EUDC test cycles. *Sci. Total Environ.* **2013**, *445*, 110–116. [CrossRef]
41. Wu, D.; Ding, X.; Li, Q.; Sun, J.; Huang, C.; Yao, L.; Wang, X.; Ye, X.; Chen, Y.; He, H.; et al. Pollutants emitted from typical Chinese vessels: Potential contributions to ozone and secondary organic aerosols. *J. Clean. Prod.* **2019**, *238*, 117862. [CrossRef]
42. Sindelarova, K.; Granier, C.; Bouarar, I.; Guenther, A.; Tilmes, S.; Stavrakou, T.; Müller, J.F.; Kuhn, U.; Stefani, P.; Knorr, W. Global data set of biogenic VOC emissions calculated by the MEGAN model over the last 30 years. *Atmos. Chem. Phys.* **2014**, *14*, 9317–9341. [CrossRef]

43. Gao, J.; Zhang, J.; Li, H.; Li, L.; Xu, L.; Zhang, Y.; Wang, Z.; Wang, X.; Zhang, W.; Chen, Y.; et al. Comparative study of volatile organic compounds in ambient air using observed mixing ratios and initial mixing ratios taking chemical loss into account—A case study in a typical urban area in Beijing. *Sci. Total Environ.* **2018**, *628*, 791–804. [CrossRef]
44. Yang, X.; Xue, L.; Yao, L.; Li, Q.; Wen, L.; Zhu, Y.; Chen, T.; Wang, X.; Yang, L.; Wang, T.; et al. Carbonyl compounds at Mount Tai in the North China Plain: Characteristics, sources, and effects on ozone formation. *Atmos. Res.* **2017**, *196*, 53–61. [CrossRef]
45. Liu, T.; Hong, Y.; Li, M.; Xu, L.; Chen, J.; Bian, Y.; Yang, C.; Dan, Y.; Zhang, Y.; Xue, L.; et al. Atmospheric oxidation capacity and ozone pollution mechanism in a coastal city of southeastern China: Analysis of a typical photochemical episode by an observation-based model. *Atmos. Chem. Phys.* **2022**, *22*, 2173–2190. [CrossRef]
46. Khan, M.A.H.; Cooke, M.C.; Utembe, S.R.; Archibald, A.T.; Derwent, R.G.; Jenkin, M.E.; Morris, W.C.; South, N.; Hansen, J.C.; Francisco, J.S.; et al. Global analysis of peroxy radicals and peroxy radical-water complexation using the STOCHEM-CRI global chemistry and transport model. *Atmos. Environ.* **2015**, *106*, 278–287. [CrossRef]
47. Onel, L.; Brennan, A.; Seakins, P.W.; Whalley, L.; Heard, D.E. A new method for atmospheric detection of the CH_3O_2 radical. *Atmos. Meas. Tech.* **2017**, *10*, 3985–4000. [CrossRef]
48. Zhao, W.; Tang, G.; Yu, H.; Yang, Y.; Wang, Y.; Wang, L.; An, J.; Gao, W.; Hu, B.; Cheng, M.; et al. Evolution of boundary layer ozone in Shijiazhuang, a suburban site on the North China Plain. *J. Environ. Sci.* **2019**, *83*, 152–160. [CrossRef] [PubMed]
49. Wang, M.; Chen, W.; Zhang, L.; Qin, W.; Zhang, Y.; Zhang, X.; Xie, X. Ozone pollution characteristics and sensitivity analysis using an observation-based model in Nanjing, Yangtze River Delta Region of China. *J. Environ. Sci.* **2020**, *93*, 13–22. [CrossRef] [PubMed]
50. Liu, Y.; Shao, M.; Fu, L.; Lu, S.; Zeng, L.; Tang, D. Source profiles of volatile organic compounds (VOCs) measured in China: Part I. *Atmos. Environ.* **2008**, *42*, 6247–6260. [CrossRef]
51. Zhang, Y.; Wang, X.; Zhang, Z.; Lü, S.; Huang, Z.; Li, L. Sources of C2–C4 alkenes, the most important ozone nonmethane hydrocarbon precursors in the Pearl River Delta region. *Sci. Total Environ.* **2015**, *502*, 236–245. [CrossRef] [PubMed]
52. Lee, J.D.; Drysdale, W.S.; Finch, D.P.; Wilde, S.E.; Palmer, P.I. UK surface NO2 levels dropped by 42% during the COVID-19 lockdown: Impact on surface O_3. *Atmos. Chem. Phys.* **2020**, *20*, 15743–15759. [CrossRef]
53. Wang, Y.; Bastien, L.; Jin, L.; Harley, R.A. Responses of Photochemical Air Pollution in California's San Joaquin Valley to Spatially and Temporally Resolved Changes in Precursor Emissions. *Environ. Sci. Technol.* **2022**, *56*, 7074–7082. [CrossRef] [PubMed]
54. Hui, L.; Liu, X.; Tan, Q.; Feng, M.; An, J.; Qu, Y.; Zhang, Y.; Jiang, M. Characteristics, source apportionment and contribution of VOCs to ozone formation in Wuhan, Central China. *Atmos. Environ.* **2018**, *192*, 55–71. [CrossRef]